



Original Paper

Geochemistry and heterogeneous accumulation of organic matter in lacustrine basins: A case study of the Eocene Liushagang Formation in the Fushan Depression, South China Sea



Bang Zeng^a, Mei-Jun Li^{a, b, *}, Ning Wang^{b, **}, Yang Shi^c, Fang-Zheng Wang^a, Xin Wang^a

^a State Key Laboratory of Petroleum Resources and Prospecting, College of Geosciences, China University of Petroleum (Beijing), Beijing, 102249, China

^b Key Laboratory of Exploration Technologies for Oil and Gas Resources, Ministry of Education, College of Resources and Environment, Yangtze University, Wuhan, Hubei, 430100, China

^c Southern Oil Exploration and Development Company, PetroChina, Haikou, Hainan, 570216, China

ARTICLE INFO

Article history:

Received 21 December 2021

Received in revised form

2 March 2022

Accepted 26 July 2022

Available online 9 August 2022

Edited by Jie Hao and Teng Zhu

Keywords:

Organic matter

Geochemical characteristics

Heterogeneous accumulation

Areal distribution

Lacustrine basin

ABSTRACT

Determining the spatial distributions of organic-rich mudstones in hydrocarbon-bearing lacustrine basins is crucial for targeting exploration wells and discovering commercially viable petroleum accumulations. However, the strong heterogeneity of sedimentary systems and organic matter (OM) input and accumulations make it difficult to identify OM-rich mudstones in lacustrine deposits. This paper takes the Eocene Liushagang Formation, in the Fushan Depression, South China Sea, as an example to clarify the relationship between the geochemical characteristics of OM and sedimentary facies. A practical approach is proposed for predicting the spatial distribution of good-quality source rocks with high OM contents. The method used is a combination of logging-based surface fitting and the mudstone to stratum thickness ratio (M/S ratio) of different depositional systems. It was found that this approach improved TOC content prediction both vertically and laterally. The results suggest that semi-deep lacustrine mudstones with predominantly aquatic organism input, deposited in suboxic-anoxic saline stratified water, contain more preserved OM than other mudstones. Using this method, limited areas on the southern slope of the lower Liushagang sequence (SQs3), the central part of the Huangtong Sag in the middle Liushagang sequence (SQs2), and the northern part of the Huangtong Sag in the upper Liushagang sequence (SQs1) are determined to be the best-quality source rocks in the development area. © 2022 The Authors. Publishing services by Elsevier B.V. on behalf of KeAi Communications Co. Ltd. This is an open access article under the CC BY-NC-ND license (<http://creativecommons.org/licenses/by-nc-nd/4.0/>).

1. Introduction

Organic-rich mudstones are the most common as source rocks in petroleum and natural gas systems (Tissot and Welte, 1984; Peters, 1986; Hunt, 1996). Hydrocarbons generated in active mudstone source rocks are relatively likely to accumulate in local traps in the same geographic location as their sources (Magoon, 2004), so defining the spatial distribution and properties of organic-rich mudstones is critical for locating commercial

hydrocarbon accumulations. Numerous studies have examined the accumulation and geochemical characteristics of OM across geological time within the sequence stratigraphic framework (Bohacs et al., 2000; Peters et al., 2000; Lai et al., 2018, 2020a, 2020b, 2020c; Li et al., 2018; Makled et al., 2018; Fu et al., 2022), describing the vertical variability of OM with reasonable accuracy. However, few studies have focused on the lateral heterogeneity of OM within the sedimentary framework (Lai et al., 2020c), resulting in an inadequate understanding of the areal distribution of organic-rich mudstones. There are two main reasons for this: (1) the relative scarcity of exploratory wells in suitable source rocks means that the available samples are limited in quality and distribution; (2) appropriate parameters have not yet been established for determining the relationship between geochemical characteristics and sedimentary facies. Conventional organic geochemical analysis employs only a limited selection of data points to describe the

* Corresponding author. State Key Laboratory of Petroleum Resources and Prospecting, College of Geosciences, China University of Petroleum (Beijing), Beijing, 102249, China.

** Corresponding author.

E-mail addresses: meijunli@cup.edu.cn, meijunli2008@hotmail.com (M.-J. Li), cupwangning@outlook.com (N. Wang).

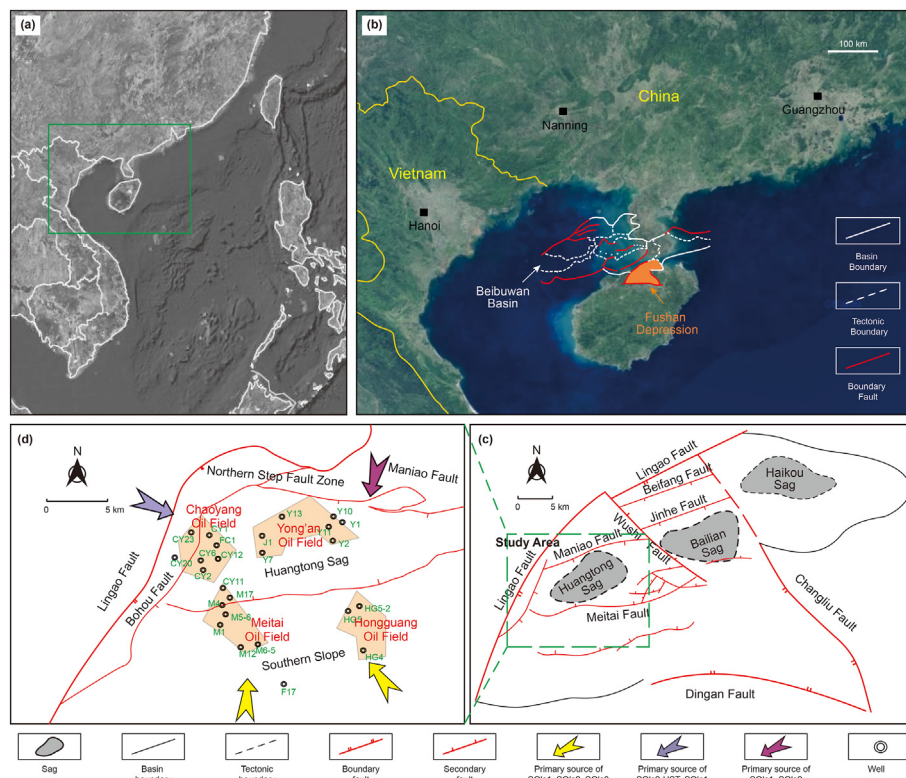


Fig. 1. (a) and (b) Maps showing the location of the Fushan Depression (after Zhang et al., 2013). (c) Structural division of the Fushan Depression (after Gan et al., 2020). (d) Sketch map of the western region of the Fushan Depression. Primary sediment source directions are from Li et al., (2017).

organic geochemical properties of source rocks, which tends to conceal their heterogeneity (Al-atta et al., 2014; Sheikh et al., 2016; Ndip et al., 2019). It is therefore imperative to develop a model that can describe variations in the spatial distribution of OM as well as its geochemical properties.

Continuous logging data has been used by geologists since the 1970s to estimate the organic richness of mudstones (Schmoker, 1979; Fertl and Chilingar, 1988; Passey et al., 1990; Bodin et al., 2011; Wang et al., 2016). In recent years, although advances in computer technology have markedly improved the accuracy of geochemical parameter prediction in individual wells (Mahmoud et al., 2017; Yu et al., 2017; Wang et al., 2019; Bai and Tan, 2020; Zeng et al., 2021), the difficulty in describing the areal heterogeneity of OM has not been addressed. Løseth et al. (2011) proposed a seismic-based method to identify, characterize, and map the distribution and variations of OM. However, the high-quality requirements and relatively low resolution of seismic data restrict the application and utility of this method. Geophysical methods such as this are often not correlated with geological theory and the known geological background of specific locations, resulting in erroneous conclusions in many cases.

There is a large number of hydrocarbon-rich rift depressions filled with lacustrine deposits in eastern China, such as the Bohong (Yin et al., 2020) and Dongying Depressions (Zou et al., 2018) in the Bohai Bay Basin, and the Gulong Depression in the Songliao Basin (Liu et al., 2018). The sediments in these basins show strong heterogeneity in minerals, lithology, and organic geochemical characteristics (Jiang et al., 2017; Liu et al., 2018; Lai et al., 2020c). The Fushan Depression is a typical Cenozoic lacustrine unit in the Beibuwan Basin (Liu et al., 2015). Obvious differences in the physical properties and geochemical characteristics of crude oils from different structural units in the depression indicate a variety of OM

sources (Lu et al., 2016; Gan et al., 2020; Shi et al., 2020). However, despite this, the spatial distribution and characteristics of organic-rich mudstones have not been studied. In addition, the apparent multi-directionality of the depression's provenance system presents considerable challenges to the study of OM accumulation (Li et al., 2017).

Sedimentary facies vary consistently in the vertical and lateral sections. If the relationships between geochemical parameters and sedimentary facies are correctly understood, areal geochemical characteristics of OM can be inferred from data from individual wells. In this study, a new method for revealing areal variations in TOC content is proposed based on a combination of organic geochemistry, geophysics, and sedimentology. OM enrichment models are proposed for different sets of mudstones from the Eocene Liushangang Formation and the spatial distributions of organic-rich mudstones determined within the sequence stratigraphic framework. The results will have considerable practical value for identifying and prioritizing exploration targets in the field. This is a novel and practical method with wide general applicability for source rock evaluation in lacustrine basins.

2. Geological background

The Fushan Depression, situated in the south part of the Beibuwan Basin (Fig. 1a and b), is one of a number of Mesozoic-Cenozoic rifted half-grabens in the South China Sea. It is a NE–E trending depression, with an area of approximately 2920 km², bounded by the Lingao fault to the northwest, the Changliu fault to the northeast, and the Ding'an fault to the south (Fig. 1c). A structural transition zone in the central region separates the depression into the Baolian Sag in the east and the Huangtong Sag in the west, each of which has its own structural style and sedimentary pattern

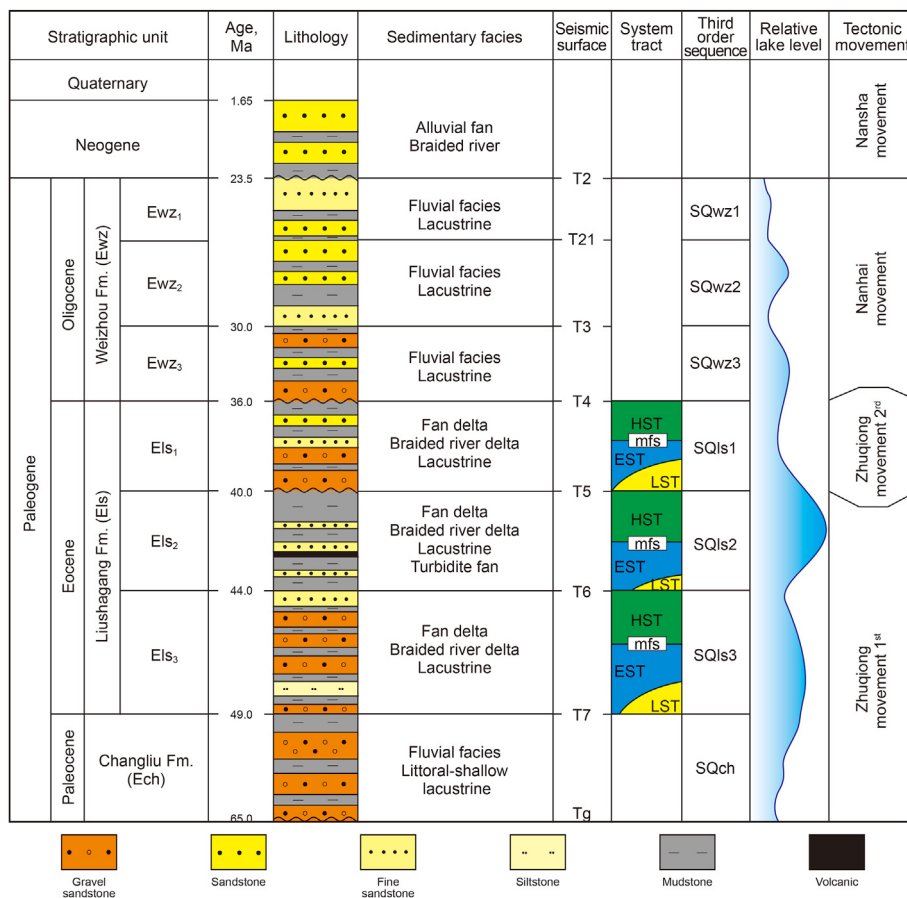


Fig. 2. Stratigraphic column and sequence division of the Fushan Depression (after Gan et al., 2020). The relative lake level is from Liu et al. (2014). LST, lowstand systems tract; EST, transgressive systems tract; HST, highstand systems tract.

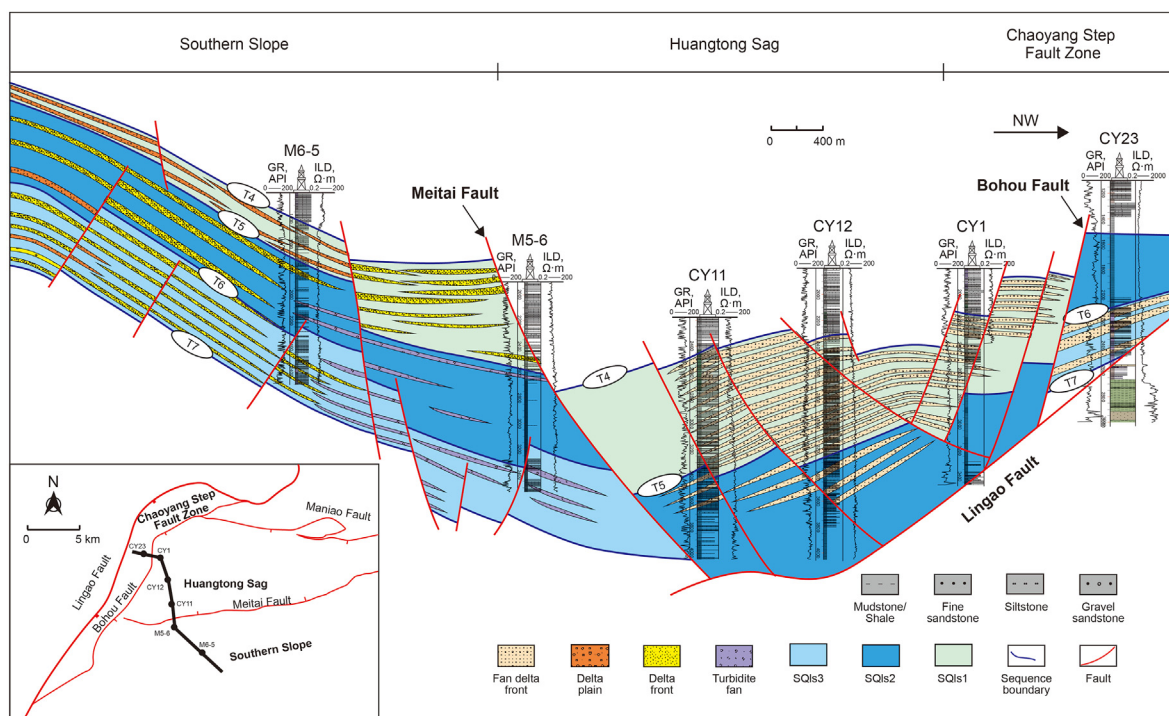


Fig. 3. Well-correlation section showing the sedimentary characteristics and evolution.

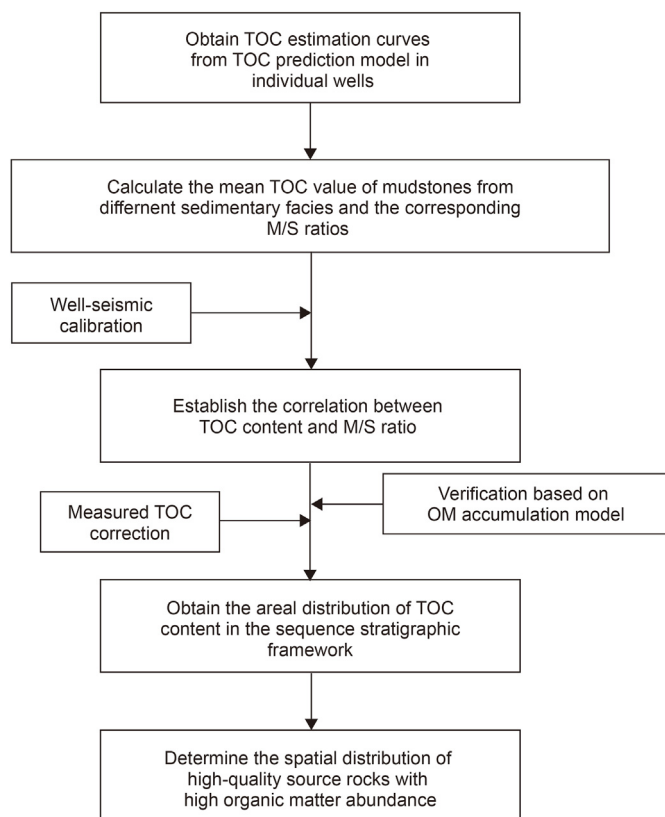


Fig. 4. Workflow for obtaining the spatial distribution of organic-rich mudstones in lacustrine basins.

(Liu et al., 2014). This study focuses on the western region of the Fushan Depression, as shown on the sketch map in Fig. 1d. There are three tertiary structural units in the western region: the northern step fault zone, the central Huangtong Sag, and the southern slope zone (from north to south).

There are Cenozoic sediments over 9000 m thick in the Fushan Depression. The depression can be divided into the Paleocene Changliu Formation, the Eocene Liushagang Formation, the Oligocene Weizhou Formation, and the Neogene strata (from the bottom to top). The Liushagang Formation is considered to be the major oil-bearing layer. This formation is sub-divided into three members—Els₃, Els₂ and Els₁—which correspond to the SQIs3, SQIs2 and SQIs1 sequences, respectively (Fig. 2) (Liu et al. 2012, 2014; Ma et al., 2012). Major boundary faults, which formed during deposition of the formation (Li et al., 2008), controlled its sedimentary evolution, resulting in a multi-directional provenance system. Sediments from the northern provenance formed fan delta facies in the step fault zone. Braided river delta facies supplied from the southern provenance developed widely in the slope zone. Lacustrine facies and turbidite fans composed of dark mudstones and siltstone intervals formed in the central Huangtong Sag (Li et al., 2017). The sedimentary facies characteristics and evolutionary history are shown in Fig. 3.

3. Materials and methods

3.1. Materials

A total of 81 core samples and 115 cutting samples were collected from 21 wells for total organic carbon (TOC) content analysis and Rock-eval pyrolysis experiments. All the samples were

obtained from mudstone layers within the Liushagang Formation. The locations of the sampling wells are shown in Fig. 1d. Twenty-five samples were selected for further OM extraction and gas chromatography (GC) – mass spectrometry (MS) analysis. Twenty-five well-logging curves were collected for mudstone classification and TOC estimation. Maps of the sedimentary facies and M/S ratio isolines were obtained from the Fushan Oilfield, PetroChina.

3.2. Geochemical experiments

All the samples were crushed to 80 mesh powder (diameter less than 2 mm) and washed with deionized water to remove residual contamination. TOC contents were measured using a LECO CS-230 carbon analyzer, following removal of carbonates by dilute hydrochloric acid (1.5 mol/L). The Rock-eval pyrolysis experiments were carried out using an OGE-VI rock pyrolyzer. Ground samples, each weighing 100 mg, were heated to 600 °C to measure the Rock-Eval parameters (S₁: volatile hydrocarbon content, S₂: remaining hydrocarbon generation potential, T_{max}: temperature at maximum pyrolysis yield). (Table S1).

Twenty-five powdered samples (each 100 g) from different sedimentary environments were extracted using a Soxhlet apparatus, operated for 48 h with dichloromethane and methanol as the solvents (93:7, volume: volume). The extracts were then deasphalted using n-hexane and separated by liquid chromatography to obtain saturate, aromatic, and resin fractions. GC–MS analysis of the saturated hydrocarbon fractions was conducted using an Agilent 6890 gas chromatograph coupled to an Agilent 5975i mass selective detector. An HP-5 MS fused silica capillary column was used for separation, with helium as the carrier gas. The GC oven temperature was initially set at 50 °C, ramped to 120 °C at a rate of 20 °C/min, then raised to a final temperature of 310 °C at 3 °C/min. The MS was operated in electron impact mode with an ionization energy of 70 eV and a scanning range of 50–600 Da.

3.3. Prediction of spatial distribution of organic-rich mudstones

Zeng et al. (2021) proposed a logging-based TOC prediction model for the extensive organic-rich mudstone interlayers in the Fushan Depression using surface fitting (Fig. 3). The model was adopted in this study to evaluate vertical variations in TOC content. TOC prediction curves for 25 wells were obtained, and the mean TOC values of mudstones from different sedimentary facies in individual wells are listed in Table S2. Sedimentary facies were identified using lithology logging and conventional logging curves (Liu et al., 2014; Liao et al., 2015). Well-seismic calibration was used to correct for strata thickness. Then, the M/S ratio was utilized as a bridge between the sedimentary facies and geochemical parameters to construct a mathematical relationship with TOC content, which will facilitate accurate description of the lateral distribution of OM. OM accumulation models were used to verify that the mathematical relationship conforms to geological theory. Finally, the areal TOC content distribution was determined from contour maps of the M/S ratio, corrected using measured TOC values. The specific workflow is shown in Fig. 4.

4. Results

4.1. Mudstone classification based on sedimentary subfacies

OM accumulation is essentially controlled by the sedimentary environment and the preservation and productivity conditions it provides (Demaison and Moore, 1980; Pedersen and Calvert, 1990; Sageman et al., 2003; Mort et al., 2007). Based on the depositional characteristics of the Liushagang Formation, a total of six types of

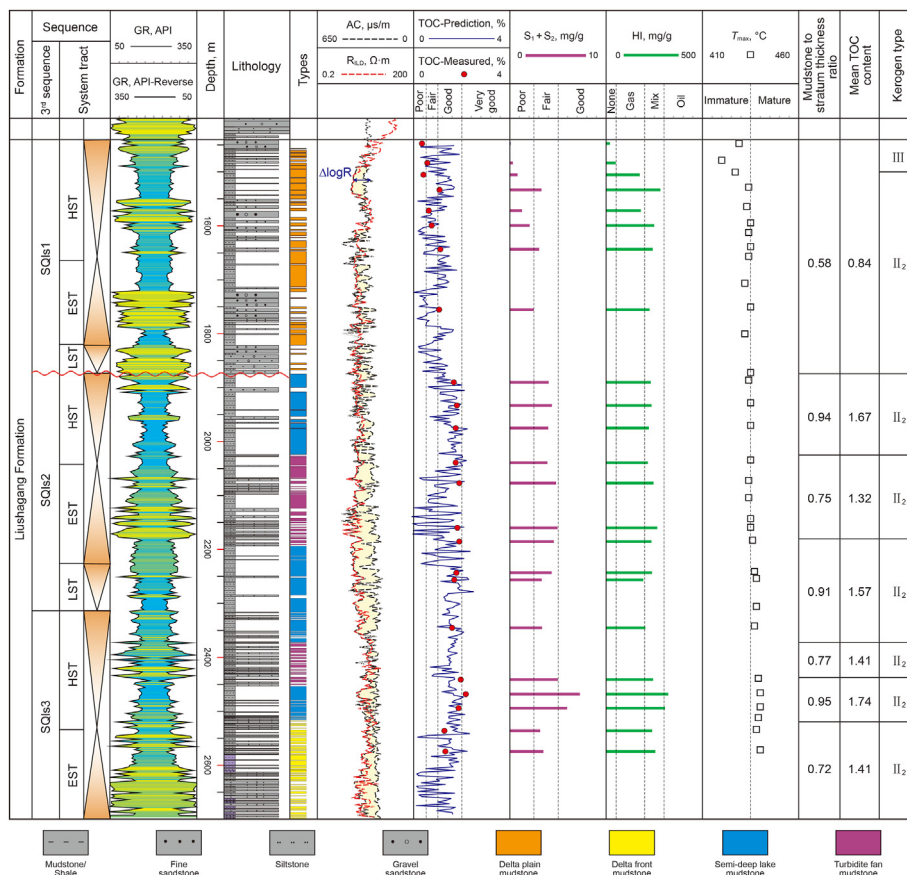


Fig. 5. Profiles of geochemical characteristics and conventional logging curves of well M6-5.

mudstones are distinguished: (1) Delta plain mudstones (DPM), which originated in a braided river deltaic plain environment. Their lithology is minor maroon-to grey-colored mudstone interlayers in thick deltaic sandstones, and they have medium amplitude box-shaped natural gamma ray (GR) logging curves (Fig. 5). The M/S ratios are less than 0.6. (2) Delta front mudstones (DFM), which come from braided river delta front facies. Their GR curves are bell- and funnel-shaped, and their M/S ratios are about 0.6–0.8 (Fig. 5). (3) Shallow lake mudstones (SLM), such as light grey-colored or silty mudstones deposited in a shallow-water environment. The M/S ratios range from 0.8 to 0.9. (4) Semi-deep lake mudstones (SDLM), which were deposited in a deep-water environment and have M/S ratios higher than 0.9. Their lithology is predominantly thick dark mudstones, with occasional interbedded siltstone and their GR curves are low amplitude linear shapes (Figs. 5 and 6). (5) Fan delta front mudstones (DFDM) from a fan deltaic depositional environment. These mudstones are multistage and stacked vertically with gravel sandstones. The M/S ratios are about 0.5–0.8 and the GR curves show medium-to low-amplitude serrated bell- and box-shapes (Fig. 6). (6) Turbidite fan mudstones (TBFM), which were deposited in a relatively deep-water environment. The lithology is dark, massive mudstones with sandstone and siltstone intervals. The M/S ratios are estimated to be between 0.6 and 0.8 and the turbidite deposits show thin, finger-shaped GR curves (Figs. 5 and 7). The real distributions of the different mudstones in the Liushagang sequences are shown in Fig. 8a, b and c.

4.2. Organic matter richness, kerogen type and hydrocarbon generation potential

TOC content and Rock-Eval pyrolysis parameters are generally

used for source rock evaluation. In this study, the TOC and potential hydrocarbon yield indices ($GP = S_1 + S_2$), the cross-plot of hydrogen indices ($HI = S_2 / TOC \times 100$) versus T_{max} , and the cross-plot of S_2 versus TOC contents were used to assess the organic matter richness, kerogen types, and hydrocarbon generation potential, respectively, of the different mudstones (Tissot and Welte, 1984; Peters, 1986; Bordenave et al., 1993; Peters and Cassa, 1994).

SDLMs show the highest abundance of OM. TOC and GP values range from 1.09%–2.19% and 0.89–7.27 mg HC/g rock, respectively, with averages of 1.64% and 3.61 mg HC/g rock (Table S1). Kerogen classification plots show that these mudstones have predominantly type I to type II₂ kerogens with relatively high HI values, ranging from 55.28 to 321.81 mg HC/g TOC (average 195.64 mg HC/g TOC) (Fig. 8g–i). The SDLM samples from the southern slope zone (mainly collected from sequences SQIs2 and SQIs3) and the Huangtong sag (mainly from sequence SQIs1) show polarized S_2 yields ranging from 2.10–6.98 mg HC/g rock (average 4.36 mg HC/g rock) and 0.83–4.12 mg HC/g rock (average 1.59 mg HC/g rock), respectively (Table S1). The higher values of TOC and S_2 of SDLMs indicate fair to good hydrocarbon generation potential (Fig. 8d and e). By contrast, other SDLM samples with medium TOC contents and lower S_2 yields have higher T_{max} and deeper burial depths (Table S1), indicating that the SDLMs from the Huangtong Sag have higher thermal maturity, resulting in poor-to-fair current hydrocarbon generation potential (Fig. 8f).

SLMs, DFMs and DFDMs have predominantly type II₁ to type II₂ kerogen (Fig. 8g–i). The TOC contents and GP range from 1.30%–1.55% (average 1.47%) and 3.17–4.71 mg HC/g rock (average 3.95 mg HC/g rock), 1.28%–1.68% (average 1.46%) and 2.84–6.03 mg HC/g rock (average 4.12 mg HC/g rock), 0.52%–1.94% (average 1.30%) and 0.49–10.44 mg HC/g rock (average 3.43 mg HC/g rock), respectively

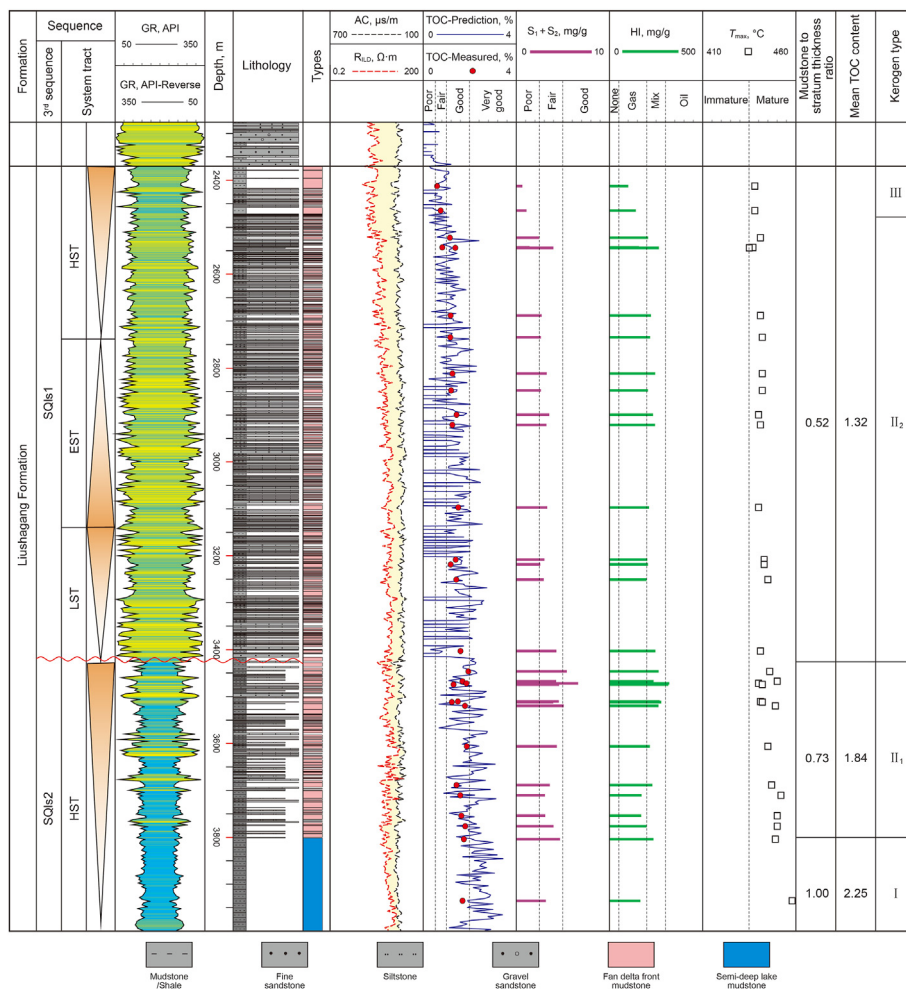


Fig. 6. Profiles of geochemical characteristics and conventional logging curves of well CY12.

(Table S1), indicating moderate OM enrichment. It is noted that the DFMs and FDFMs exhibit a wider range of organic matter richness than SLMs. Fig. 8d–f shows that these mudstones have poor-to-fair hydrocarbon generation potential.

TBFMs have medium TOC contents (0.71%–1.90%, with an average of 1.24%) and GP values (0.65–5.09 mg HC/g rock, with an average of 2.68 mg HC/g rock) (Table S1). Like the SDLMs, TBFMs from deeper depths in the Huangtong Sag, with predominantly type I to type II₂ kerogen (Fig. 8i), have lower hydrocarbon generation potential than the TBFMs in the southern slope zone (Fig. 8d–f).

The DPM samples have lower abundance of OM, with TOC ranging from 0.35% to 1.11% (average 0.83%) and GP ranging from 0.07 mg HC/g rock to 3.04 mg HC/g rock (average 1.75 mg HC/g rock) (Table S1). These mudstones contain predominantly type II₂ to type III kerogen (Fig. 8i) and are classified as poor source rocks according to the cross-plot of S₂ versus TOC (Fig. 8f).

4.3. Biomarker compositions

4.3.1. n-Alkanes and isoprenoids

The biomarker compositions of mudstones (e.g., n-alkanes, isoprenoids, hopanes, and steranes) provide information about their depositional environments and OM sources (Eglinton and Hamilton, 1967; Huang and Meinschein, 1979; Peters et al., 2005). In this study, the n-alkane series in all samples ranges from nC₁₃ to

nC₃₅. Total ion chromatograms (TIC) for the saturated hydrocarbon fractions of mudstones supplied from the southern provenance (e.g., DFM, SLM and TBFM from the southern slope zone) are unimodal, with maxima at nC₂₇ (Fig. 9a and b, TIC). In contrast, samples predominantly supplied from the northern provenance system (e.g., FDFM and TBFM from the northern step fault zone) show bimodal n-alkane distributions with a predominance of nC₁₆ and nC₂₇ (Fig. 9e and f, TIC). SDLM extracts display a unimodal n-alkane distribution with a strong preference for carbon numbers between nC₁₈ – nC₂₁ (Fig. 9c and d, TIC). Most mudstone extracts show a weak odd-carbon preference in the range of nC₂₅ (1.03 < CPI < 1.49, average 1.13, 0.86 < OEP < 1.22, average 1.05), while other samples from depths of less than 2000 m have a more marked odd-carbon preference (1.93 < CPI < 2.46, 1.29 < OEP < 2.12), indicating lower thermal maturity and greater terrigenous high plant input (Peters et al., 2005). Pristane (Pr)/phytane (Ph) ratios range from 1.08 to 5.82 (Table S3), indicating that sub-oxic to oxic conditions prevailed during the Eocene period.

4.3.2. Tricyclic terpanes and hopanes

A series of tricyclic terpanes (TTs) was detected in mudstone samples from the Liushagang Formation. A number of previous studies have pointed out that C₁₉TT and C₂₀TT are abundant in mudstones with terrigenous OM input, whereas C₂₃TT tends to predominate in marine mudstones (Peters and Moldowan, 1993; Volk et al., 2005). The m/z 191 mass chromatograms in Fig. 9a and b

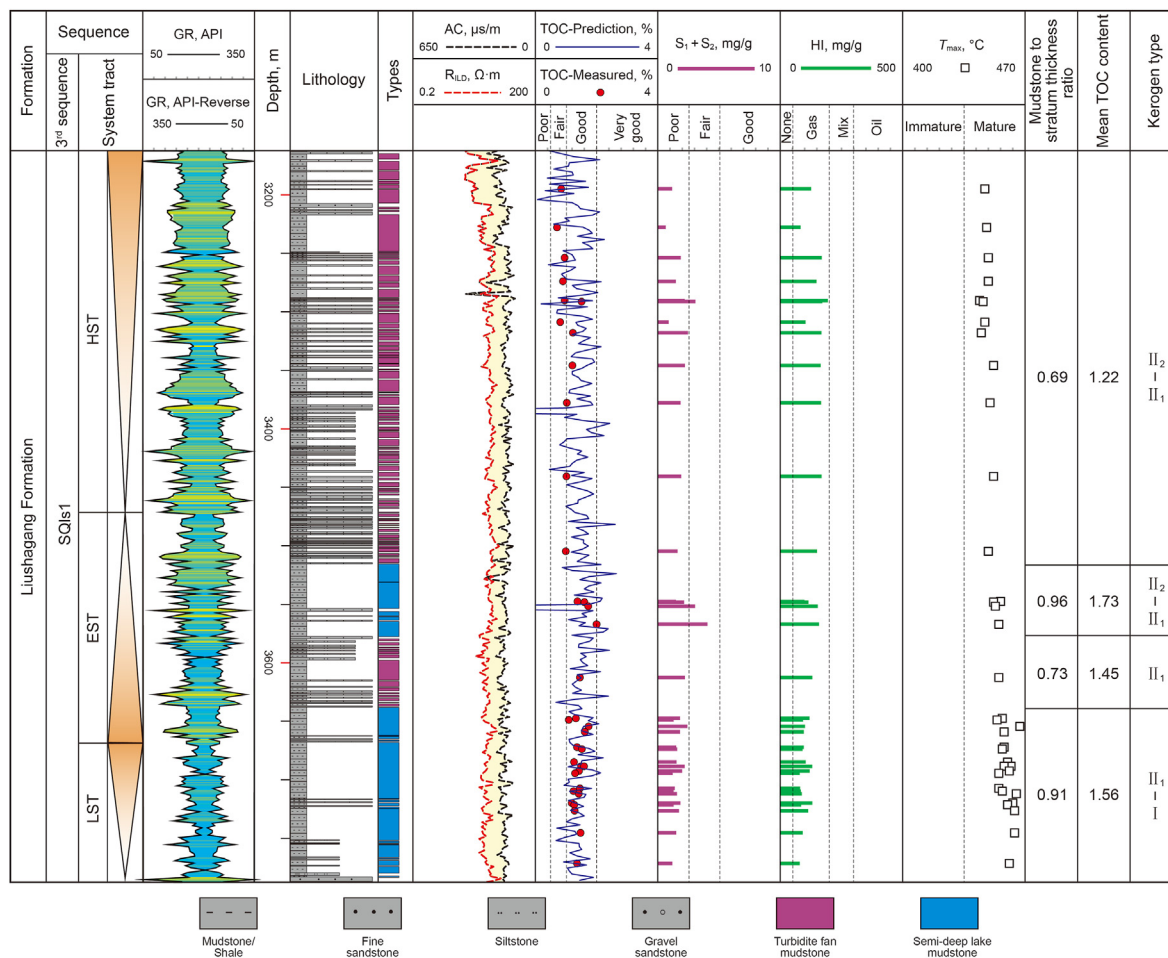


Fig. 7. Profiles of geochemical characteristics and conventional logging curves of well Y11.

shows that the DFM and SLM extracts contain relatively lower proportions of $C_{19}TT$ and $C_{20}TT$. In contrast, the $(C_{19}+C_{20})TT/C_{23}TT$ ratios are higher in the FDFM and TBFM extracts (Fig. 9e and f, m/z 191 mass chromatograms). Oleanane (OI) in OM is generally considered to originate from angiosperms such as betulin and taraxerene (Grantham and Baak, 1983; Haven and Rullkötter, 1988; Moldowan et al., 1994). The relative abundance of oleanane varies considerably between the DFM and SLM extracts and the FDFM and TBFM extracts (Fig. 9, m/z 191 mass chromatograms), suggesting that the OM sources and depositional conditions vary between the northern and southern sediments.

Gammacerane (Ga) is used a diagnostic biomarker for identifying water column stratification resulting from hypersalinity (Moldowan et al., 1985; Damsté et al., 1995). In this study, the gammacerane indices ($=Ga/C_{30}H$) of all samples are within the range 0.02–0.25 (average 0.09), indicating a fresh to brackish water depositional environment with weak water column stratification. The distribution of the homohopane series ($C_{31}H$ – $C_{35}H$) is also useful as it reflects redox conditions (Peters et al., 2005). A relatively high abundance of C_{35} hopane generally corresponds to highly reduced marine, or high-salinity lacustrine, conditions (Peters and Moldowan, 1991; Hao et al., 2011). In the mudstones of the Liushagang Formation, the homohopane series show a gradually decreasing distribution pattern from $C_{31}H$ to $C_{35}H$ (Fig. 9, m/z 191 mass chromatograms), which further implies a fresh to brackish lacustrine depositional setting.

4.3.3. Steranes

Steranes are derived from sterols in eukaryotes and represent an important biomarker type (Peters et al., 2005). C_{27} , C_{28} and C_{29} regular steranes or diasteranes are the most common sterane homologues in the saturated hydrocarbon fractions. It is generally accepted that C_{27} steranes are derived from the cellular membranes of vertebrates, algae, and plankton (Gagosian et al., 1980; Smith et al., 1982), that C_{28} steranes originate from vitamin D precursors (Gomis et al., 2000) and ergosterols (Volkman et al., 1999) synthesized by microalgae, and that C_{29} steranes are derived from sitosterol or stigmasterol precursors synthesized in higher plants (Hartmann, 1998; Peters et al., 2005). In this study, the C_{27} , C_{28} and C_{29} - $5\alpha(H)$, $14\alpha(H)$, $17\alpha(H)$ -20R-cholestanes in DFM and SLM extracts show inverted “L” shapes (Fig. 9a and b, m/z 217 mass chromatograms), with C_{29}/C_{27} regular sterane ratios higher than 1.3 (range 1.36–2.12, average 1.72), suggesting that these mudstones contain mostly terrigenous OM. In contrast, other samples (e.g., SDLM, FDFM and TBFM samples from the northern step fault zone) exhibit approximately “V” or “L” shaped distributions of C_{27} , C_{28} and C_{29} - $5\alpha(H)$, $14\alpha(H)$, $17\alpha(H)$ -20R-cholestanes (Fig. 9c–f, m/z 217 mass chromatograms), with their C_{29}/C_{27} regular sterane ratios being lower than those of DFMs and SLMs (range 0.54–1.22, average 0.93), indicating input from a mixture of lower organisms and terrigenous higher plants.

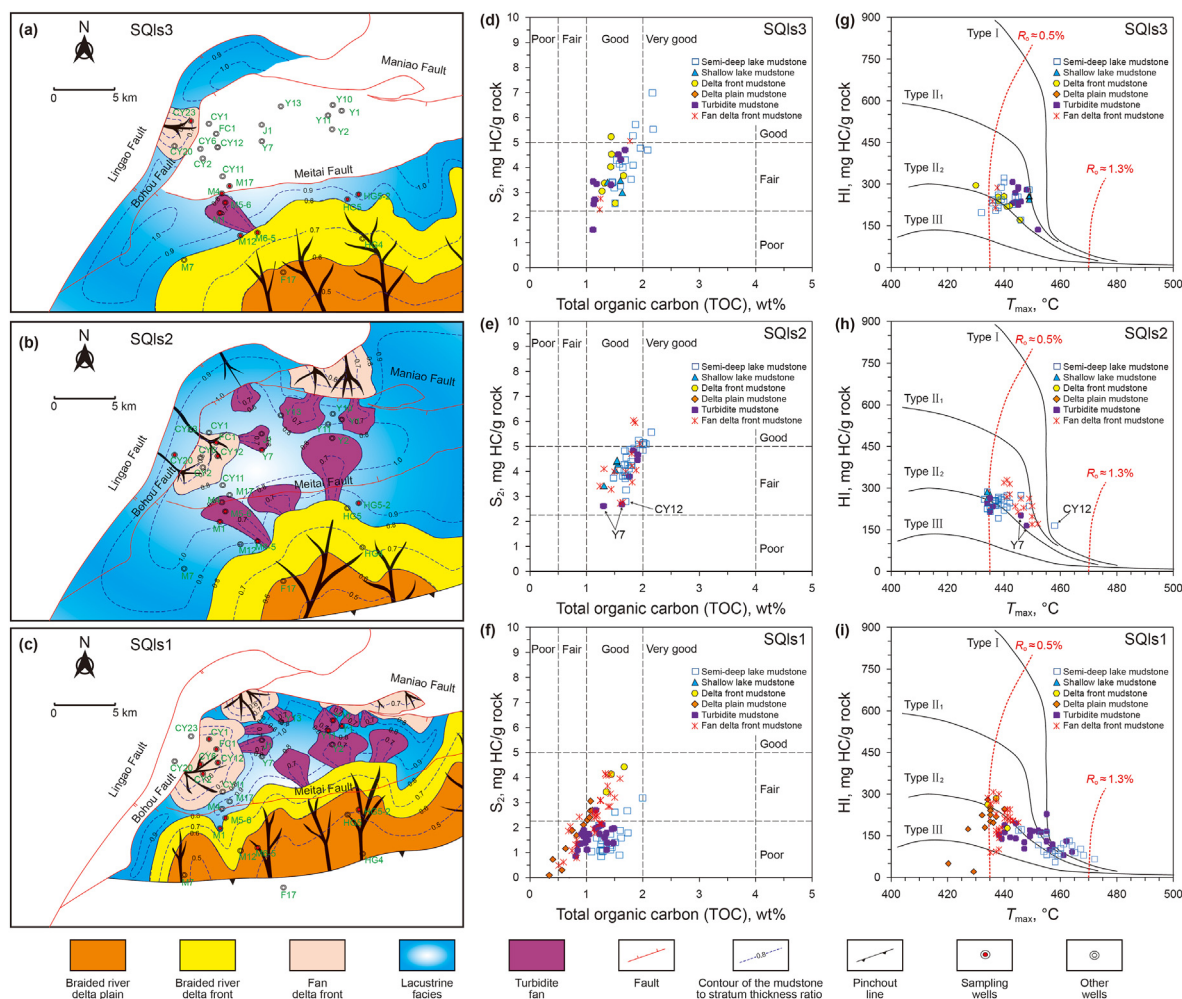


Fig. 8. (a)–(c) Maps showing the distribution of sedimentary facies and the contours of M/S ratios of different sequences of the Liushagang Formation in the western region of the Fushan Depression. (d)–(f) Cross-plot of S_2 versus TOC content of mudstone samples. (g)–(i) Cross-plot of HI versus T_{max} of mudstones.

5. Discussion

5.1. Accumulation models of organic matter in different mudstones

Geological factors, such as thermal maturity and diagenesis, greatly influence the reliability of the biomarkers that are used to describe paleoenvironments and indicate OM sources (Peters, 2005). Gan et al. (2020) demonstrated that the hydrocarbon generation threshold and peak in the Fushan Depression occur at depths of approximately 2500 m ($R_o = 0.5\%$) and 4000 m ($R_o = 1.0\%$), respectively. Most of the samples in this study were collected from within this depth range, ensuring that thermal maturity did not interfere with reconstruction of the paleoenvironment. In order to reduce the interference of other geological factors, an assemblage of geochemical parameters was used to infer the deposition conditions, rather than relying on individual biomarker parameters.

5.1.1. Organic matter sources

In the study, OM sources were determined according to n-alkane, hopane, and sterane distributions. Long chain n-alkanes ($>nC_{25}$) and short chain n-alkanes ($<nC_{20}$) are commonly used as indicators of terrigenous higher plants and lower aquatic organisms, respectively (Eglinton and Hamilton, 1967; Peters et al., 2005). C_{27} steranes are relatively abundant in aquatic OM with high algal

contribution, whereas the concentrations of C_{29} steranes are higher in OM from higher plants (Huang and Meinschein, 1979; Volkman and Maxwell, 1986). Higher terrigenous/aquatic ratios (TAR) of saturated hydrocarbon fractions correspond to higher terrigenous organic input in OM (Bourbonniere and Meyers, 1996; Meyers, 1997).

The mudstones supplied from the southern provenance (e.g., DFM, SLM and TBFM from the southern slope zone) are characterized by a unimodal n-alkane distribution, with a predominance of long chain n-alkanes (Fig. 9a and b, TIC). The TAR values and C_{29}/C_{27} regular sterane ratios are higher than 1.98 and 1.3, respectively, suggesting a higher proportion of terrigenous OM input (Fig. 10). These parameters indicate that the DFMs, SLMs and TBFMs deposited in the southern slope zone predominantly contain OM from terrigenous higher plants (Fig. 11).

Extracts of FDFM and TBFM from the northern sedimentary system show a bimodal n-alkane distribution with a predominance of long chain n-alkanes over short chain n-alkanes (Fig. 9e and f, TIC). They fall within the range of mixed OM sources in the regular sterane ternary diagram (Fig. 11). Medium TAR and C_{29}/C_{27} regular sterane ratios indicate moderate terrestrial OM input (Fig. 10). However, other parameters indicate a higher input of terrestrial OM; for example, $(C_{19}+C_{20})/TT/C_{23}TT$ ratios and the oleanane index ($=OI/C_{30}H$) (Table S3). Comprehensive analysis of biomarker indicators suggests that the OM in these mudstones is a mixture of

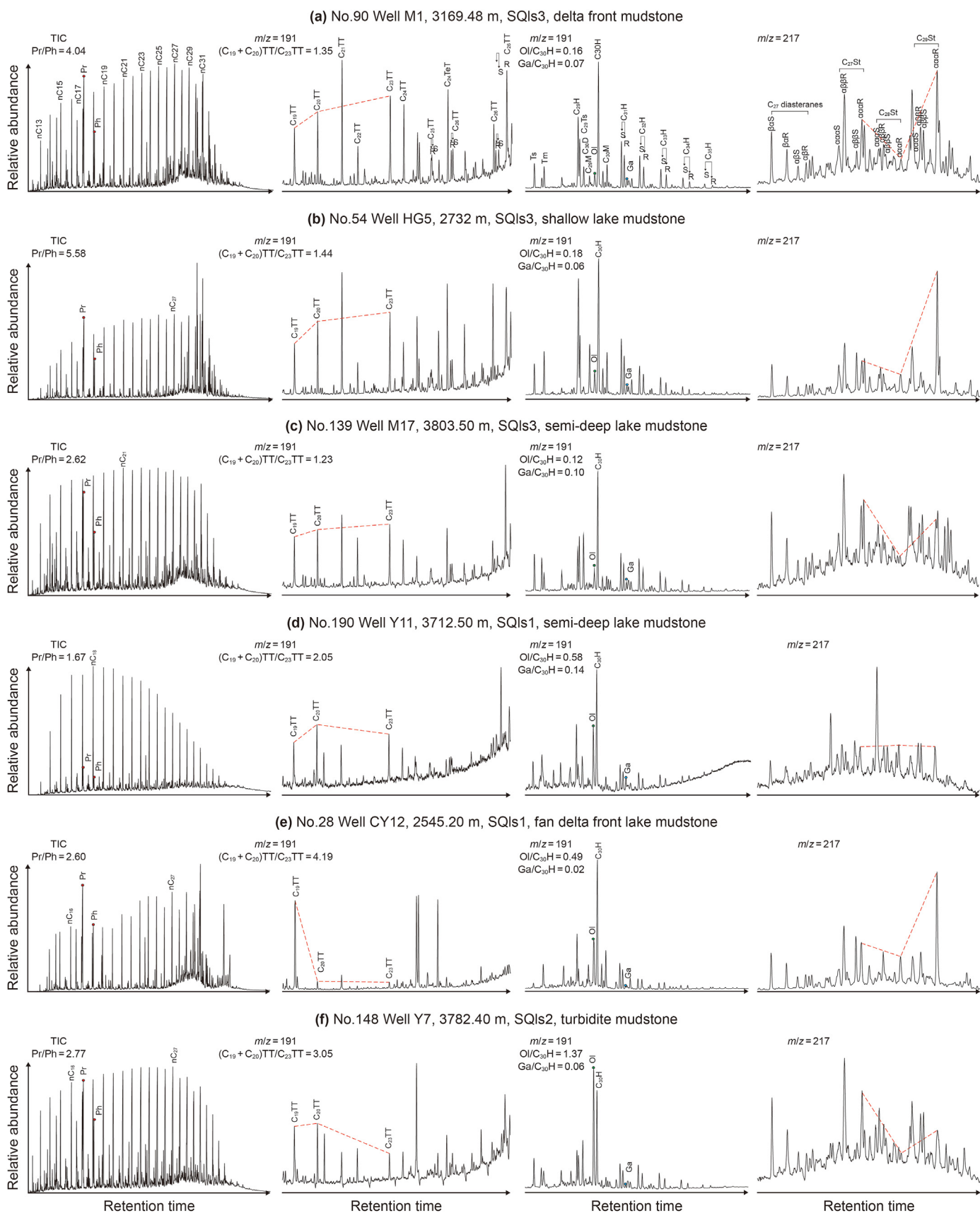


Fig. 9. Biomarker distribution of n-alkanes (TIC), terpanes (m/z 191 mass chromatograms), hopanes (m/z 191 mass chromatograms), and steranes (m/z 217 mass chromatograms) in saturated hydrocarbons of the representative mudstone extracts. Cn = C number of n-alkanes. CnTT = C number of tricyclic terpene. CnH = C number of hopane. CnSt. = C number of regular sterane. Pr = Pristane. Ph = Phytane. Ga = Gammacerane. OI = Oleanane. Tm = C₂₇ 17a-trinorhopane; Ts = C₂₇ 18a-trinorhopane.

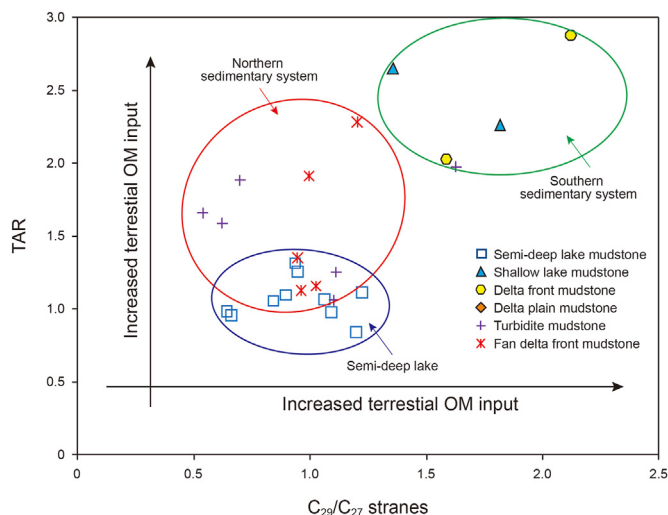


Fig. 10. Terrigenous/aquatic ratio (TAR) versus C_{29}/C_{27} regular sterane ratio showing the organic matter input. $TAR = (nC_{27} + nC_{29} + nC_{31}) / (nC_{15} + nC_{17} + nC_{19})$.

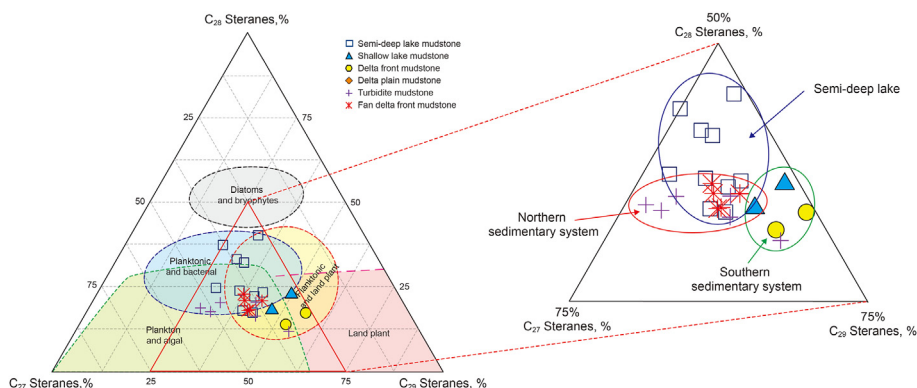


Fig. 11. Ternary diagram of regular steranes (C_{27} , C_{28} and C_{29}) showing the organic matter sources (after Huang and Meinschein, 1979).

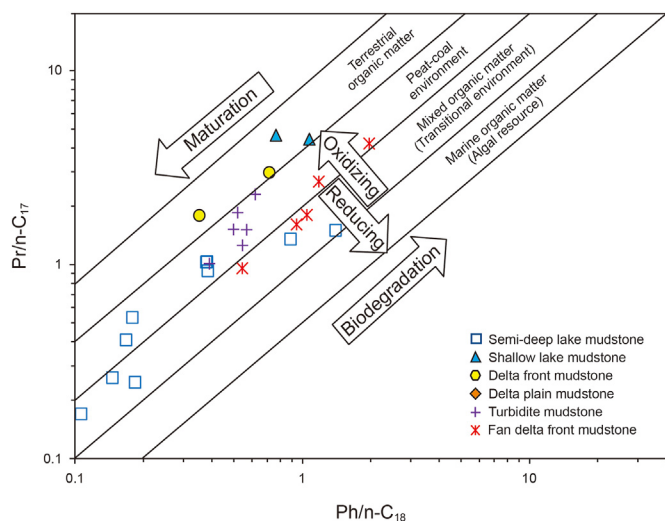


Fig. 12. Phytane to nC_{18} alkane (Ph/nC_{18}) versus Pristane to nC_{17} alkane (Pr/nC_{17}) ratios, showing deposition conditions (after Shanmugam, 1985).

bacteria, algae, and terrigenous plant material.

Total ion chromatograms of the SDLM extracts show unimodal distribution patterns of n -alkanes with the maximum varying between nC_{18} and nC_{21} (Fig. 9c and d, TIC). SDLM extracts have lower TAR and C_{29}/C_{27} regular sterane ratios than the other extracts (Fig. 10), implying less terrigenous OM input from the surrounding watershed than from aquatic sources. The OM input to these mudstones predominantly came from lower aquatic organisms, with a relatively minor contribution from terrigenous OM (Fig. 11).

5.1.2. Preservation conditions

The relative concentrations of Pr and Ph, together with Pr/nC_{17} and Ph/nC_{18} ratios and Ga indices, were used as indicators for assessing redox conditions and water column stratification (Shanmugam, 1985; Volkman and Maxwell, 1986; Peters et al., 2005). The cross plot of the Pr/nC_{17} ratio versus the Ph/nC_{18} ratio suggests that the DFMs and SLMs were formed in a terrestrial OM-dominated oxic environment, which is consistent with their higher Pr/Ph ratios (Fig. 12). The Ga index of these mudstones is lower than 0.1, another indication of oxic deposition conditions without water

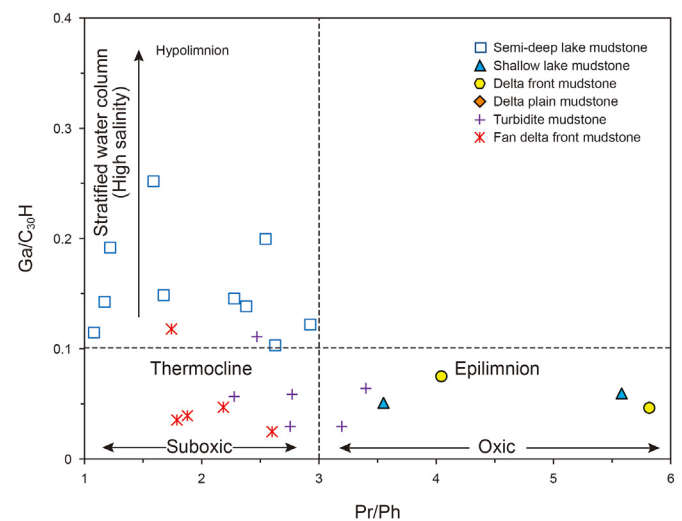


Fig. 13. The cross plot of pristane to phytane (Pr/Ph) versus gammacerane index. Epilimnion: $Ga/C_{30H} < 0.1$, $Pr/Ph > 3$. Thermocline: $Ga/C_{30H} < 0.1$, $Pr/Ph < 3$. Hypolimnion: $Ga/C_{30H} > 0.1$, $Pr/Ph < 3$.

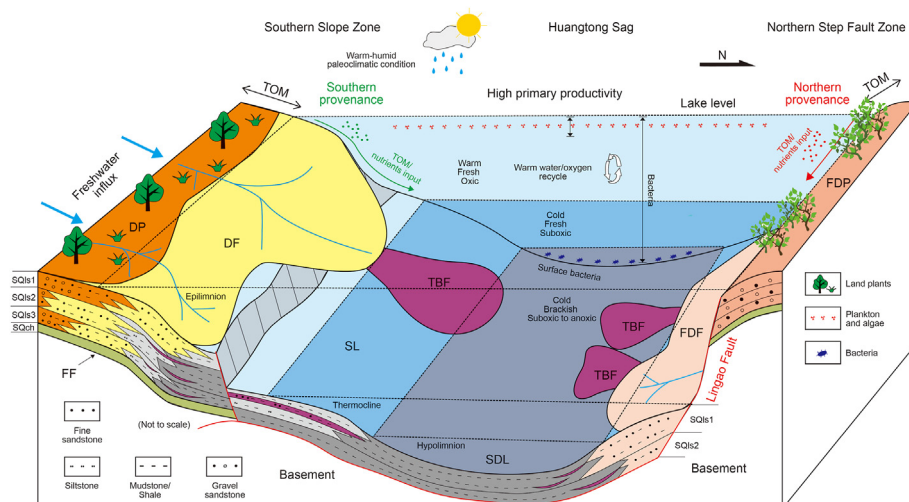


Fig. 14. Deposition and organic matter accumulation models for the Eocene Liushagang Formation. DP = Braided river delta plain. DF = Braided river delta plain front. SL = Shallow lake. SDL = Semi-deep lake. FDF = Fan delta front. FDP = Fan delta plain. TBF = Turbidite fan. FF = Fluvial facies. TOM = Terrestrial organic matter.

column stratification (Fig. 13). The Pr/Ph ratios of FDFMs and TBFMs are 1.74–2.60 (average 2.04) and 2.28–3.40 (average 2.81), respectively, falling within the range of a peat-coal environment (Fig. 12). This, combined with their lower Ga index (<0.1), suggests that they were deposited in a suboxic freshwater environment. SDLM extracts show lower Pr/Ph ratios (1.08–2.93, average 1.95) and a relatively higher Ga index (>0.1), suggesting a suboxic-anoxic brackish water depositional environment with water column stratification.

Compared with DFMs and SLMs, the depositional environments of FDFMs and TBFMs had relatively greater reducibility but similar salinity (Fig. 13). This may suggest slight water column stratification caused by temperature variations. The depositional environment of SDLMs had significantly higher salinity, resulting in better reducibility than other environments (Fig. 13). Water column stratification as a result of salinity variation probably occurred in semi-deep lacustrine environments.

5.1.3. Accumulation models

During the Eocene, a deltaic-lacustrine sedimentary system developed in the Fushan Depression. Quantitative analysis of sporopollen and clay minerals in previous studies indicated that warm, humid paleoclimatic conditions prevailed during this period (Luo et al., 2013; Li et al., 2020), causing an influx of terrestrial fresh water into the depression. Large amounts of terrestrial OM and nutrients made their way into the resulting lake through channel networks, creating favorable conditions for high primary productivity. OM accumulation models were constructed for the different types of mudstones by combining this understanding with the paleoenvironmental conditions indicated by the molecular geochemical data in this study.

The biological origins of the southern DPMs, DFMs, SLMs and TBFMs are all predominantly terrigenous OM, although the amounts and preservation conditions of the terrigenous OM inputs varied significantly between the different depositional environments. DPMs were deposited in an exposed terrestrial environment, with adequate OM input but poor preservation conditions (Fig. 14). A proportion of SLMs and DPMs are thought to have been deposited in the epilimnion, which had a higher concentration of dissolved oxygen (Figs. 13 and 14). Controlled by the sloping terrain, preservation conditions steadily improved from the delta front to the shallow lake, while the input of terrigenous OM

correspondingly reduced.

FDFMs and TBFMs supplied from the northern provenance are derived from a combination of lower aquatic organisms and terrigenous OM input. The comparatively high abundance of oleane suggests a greater input of angiosperms than in the southern provenance. Water column stratification can be induced by a thermocline in freshwater lake basins, and by a halocline in saline or brackish lake basins (Surdam and Staley, 1979; Xu et al., 2021). Most FDFMs and TBFMs are considered to have been deposited in thermoclines due to their suboxic fresh water depositional environment (Figs. 13 and 14). The marked temperature differential between the cold water at depth and the warmer water near the surface impeded the water/oxygen cycle, resulting in moderate to good preservation conditions. It is generally accepted that the deposition rate in fan delta front and turbidite fan tends to be higher than in other environments. Rapid deposition also has a positive effect on the accumulation of OM.

The water salinity apparently increased in the semi-deep lake, with a stratified water column concentrated in the area of the depocenter and forming a hypolimnion (Fig. 13). SDLMs formed in this suboxic-anoxic environment, which had the best OM preservation conditions (Fig. 14). Because of the long distance from the river mouth, only relatively small amounts of allochthonous terrigenous OM were transported to the lacustrine deep-water zone. However, primary productivity—attributed to plankton, algae, and surface bacteria—provided a greater contribution from aquatic organic material. As a result, SDLMs are characterized by higher TOC and predominantly type I to type II₂ kerogens.

5.2. Spatial distribution of organic matter

5.2.1. Areal TOC estimation models

The M/S ratio is an effective parameter for characterizing sedimentary facies (Feng, 2004). This study established the mathematical relationship between TOC content and the M/S ratio, facilitating quantitative evaluation of the areal distribution of OM (Fig. 15a).

(1) Southern sedimentary system

The TOC contents of DPMs (M/S ratio <0.6) was expected to be approximately 0.9%, with no discernible fluctuation (Fig. 15a).

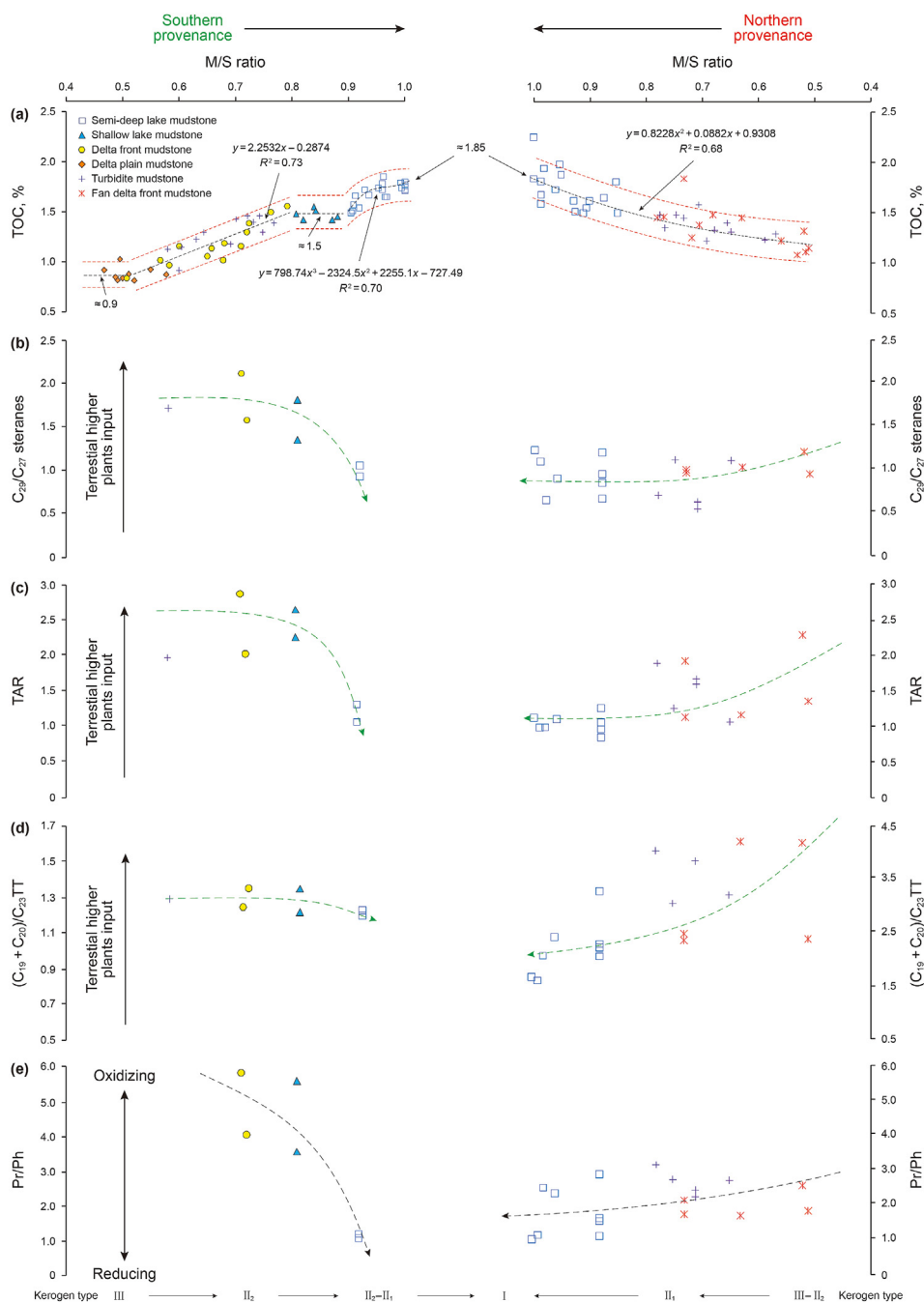


Fig. 15. (a) Variation of mean TOC content with increasing M/S ratio. (b)–(d) The cross plots of M/S ratio versus C_{29}/C_{27} regular sterane, TAR and $(C_{19} + C_{20})/C_{23}TT$, respectively, showing the variation of terrestrial OM input. (e) The cross plots of M/S ratio versus Pr/Ph showing variations in preservation conditions. R = Correlation coefficient.

Although vast amounts of OM from higher plants were deposited in-situ in the deltaic plain environment, the oxidation conditions inhibited preservation. However, terrestrial OM transported along underwater distributary channels remained stable, with M/S ratios within the range 0.6–0.8 (DFMs and TBFMs) (Fig. 15b–d), while water reducibility gradually increased (Fig. 15e), resulting in a linear increase in TOC content (Fig. 15a). Eq. (1) is the TOC estimation model for DFMs and TBFMs.

$$TOC (wt\%) = 2.2532 \times (M/S \text{ ratio}) - 0.2874 \quad (R^2 = 0.73) \quad (1)$$

The TOC of mudstones stopped increasing in shallow lake facies

($0.8 < M/S \text{ ratio} < 0.9$), with the value estimated to be 1.5% (Fig. 15a). In this setting, terrestrial OM input drastically reduced (Fig. 15b–d). However, the more reductive conditions (Fig. 15e) allowed for the preservation of a higher proportion of the inflowing OM. When the M/S ratio rose above 0.9, TOC once again increased towards the deep part of the lake, owing to the contribution of lower aquatic organisms and the salinity of the stratified water column (Fig. 15b–e). The fitting equation is set out as Eq. (2).

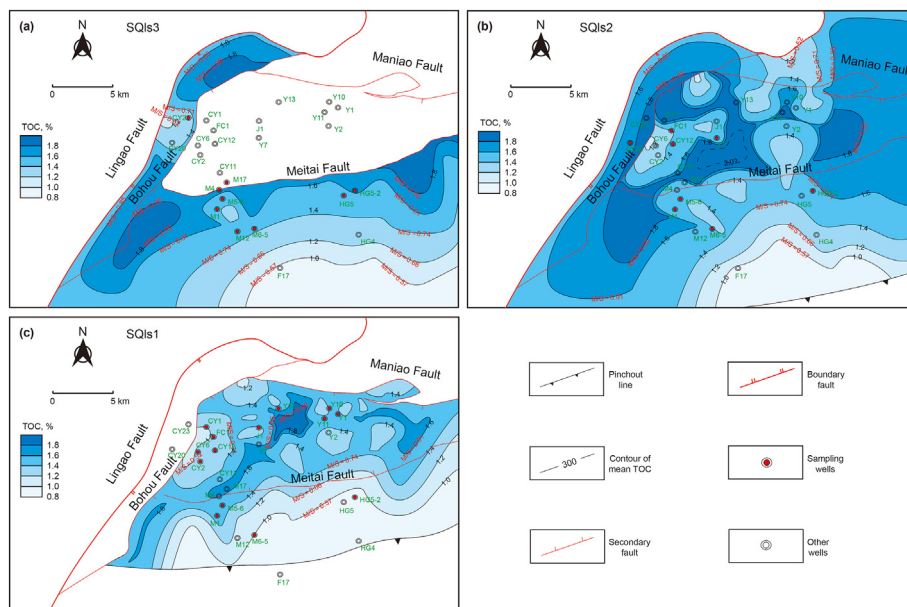


Fig. 16. Maps showing the areal TOC content of three Liushagang sequences. The isolines of TOC content were determined using the plane of M/S ratios and the prediction equations. Contour maps of the M/S ratios can be seen in Fig. 8.

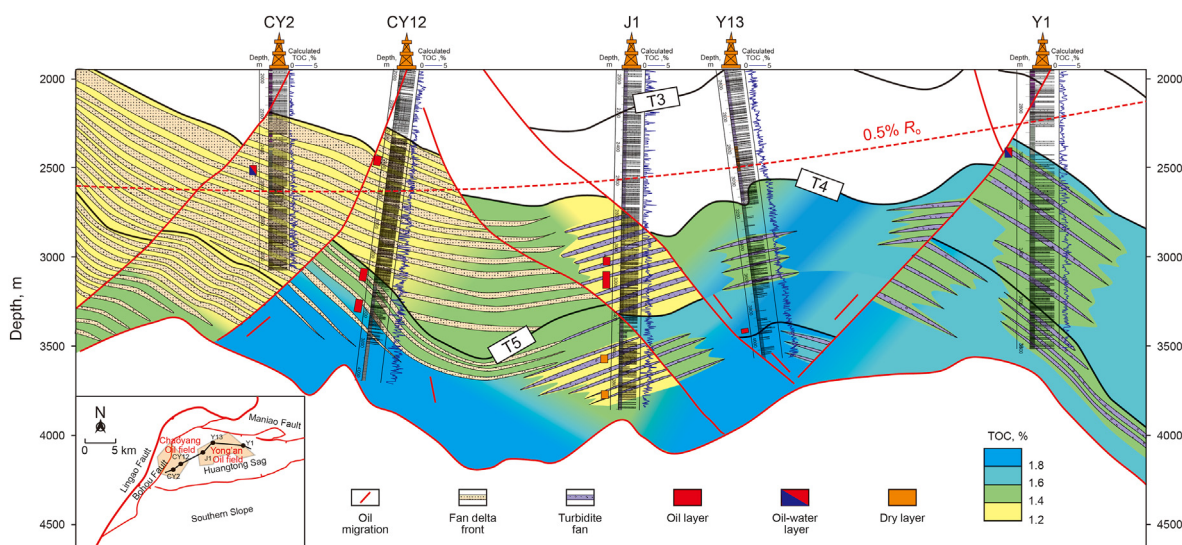


Fig. 17. Petroleum migration and accumulation model of the Yong'an and Chaoyang Oil fields.

$$\begin{aligned}
 \text{TOC (wt\%)} &= 798.74 \times (\text{M/S ratio})^3 - 2324.5 \times (\text{M/S ratio})^2 \\
 &+ 2255.1 \times (\text{M/S ratio}) - 727.49 \quad (R^2 = 0.70)
 \end{aligned}
 \tag{2}$$

(2) Northern sedimentary system

Active faults in the north Fushan Depression controlled the amount of accommodation space available for organic-rich sediment deposition, as well as the redox conditions in the bottom water, which were favorable for OM preservation (Carroll and Bohacs, 1999; Bohacs et al., 2000; Xu et al., 2021). As a result, the TOC contents of sediments deposited in the step fault zone and

central sag were relatively higher than those of the mudstones in the southern slope, showing a trend of continuous growth towards the deep lake (Fig. 15a). In areas where the M/S ratio was less than 0.7 (e.g. fan delta front and inner-middle turbidite fan subfacies), terrestrial OM input was significantly reduced from the provenance zone to the center of the lake (Fig. 15b–d), while preservation conditions were marginally improved (Fig. 15e). Nevertheless, lower aquatic organisms, such as algae and bacteria, provided sufficient supplemental organic material, resulting in increased TOC and a mixture of kerogens. Aquatic organic input almost predominated in OM deposition when the M/S ratio was greater than 0.7 (e.g. semi-deep lake, pro-fan delta, and outer turbidite fan subfacies) (Fig. 15b–d). The preservation conditions favored OM accumulation, and TOC content gradually increased towards the center of the lake. The organic richness of the mudstones in the

northern sedimentary system can be assessed using Eq. (3).

$$\text{TOC (wt\%)} = 0.8228 \times (\text{M/S ratio})^2 + 0.0882 \times (\text{M/S ratio}) + 0.9308 \quad (R^2 = 0.68) \quad (3)$$

5.2.2. Spatial distribution of organic-rich mudstones within the sequence stratigraphic framework

By combining M/S ratios, regional TOC estimation algorithms, and measured TOC correction, contour maps of the areal TOC distributions of the three Liushagang sequences were produced (Fig. 16). The mean TOC of the mudstones in the SQIs3 and SQIs2 sequences ranges from 1.0% to 2.0%, indicating that the mudstones generally meet the TOC criterion for good source rocks. Mudstones with TOC higher than 1.6% are found throughout the Huangtong Sag (Fig. 16a and b), corresponding to medium to high lake levels (Fig. 2). The SQIs1 epoch saw a dramatic drop in the lake level (Fig. 2), with deltaic and turbidite sediments predominating. The distribution of areas containing more OM shifted increasingly towards the north during this period (Fig. 16c).

There is no clear numerical relationship between OM type and the M/S ratio. However, in the southern sedimentary system, as the M/S ratio increases, the kerogen type changes from type III to type II₁, whereas, in the northern sedimentary system, it shifts from type I kerogen to type III (Figs. 5, 6 and 7).

5.3. Implications for hydrocarbon exploration

This study determines the distribution of source rocks with high OM abundance more accurately than previous studies based on an inter-well interpolation approach. This new method shows great promise for future exploration target selection. More SQIs2 oil pools have already been discovered in the Chaoyang Oilfield as a result of the plentiful high-quality source rocks identified in the SQIs2 sequence in the deep center of the Huangtong Sag (Fig. 17). In contrast, the high-quality source rock development areas in SQIs1 are mostly in the northern part of the Huangtong Sag. The oil and gas tend to migrate along faults to the much closer Yong'an Oilfield (Fig. 17). Therefore, the turbidite sand bodies in SQIs2 in the center of the Huangtong Sag and in SQIs1 in the north of the sag offer superior exploration opportunities because they are adjacent to high-quality source rocks with adequate supply.

There are two major additional benefits of the new method: (1) Using the M/S ratio enables more accurate description of the distributions of high-quality source rocks in heterogeneous lacustrine basins than has hitherto been possible, which will increase exploration success rates; (2) The technology is universally applicable, and is particularly valuable for identifying hydrocarbon sources in deeply buried strata and offshore areas. Exploration is complex, difficult and expensive in these areas, so comparatively few wells have been drilled. As a result, geological samples for source rock identification are scarce. However, M/S ratios are generally readily available, so the method outlined in this study is eminently suitable.

6. Conclusions

This study investigated the heterogeneous accumulation and characteristics of OM using an integrated sedimentological, geochemical, and geophysical approach. Three main conclusions are drawn:

- (1) The geochemical characteristics of OM are sensitive to sedimentary environment and provenance input, reflected in diverse accumulation patterns. Within the Liushagang Formation, SLMs and DFMs with predominantly terrestrial OM were deposited in the epilimnion, with moderate OM content and hydrocarbon generation ability. FDFMs and TBFMs generally formed in suboxic thermoclines with a mixture of organic materials. These are classified as fair source rocks. In contrast, the input of organic material to SDLMs developed in the hypolimnion was predominantly from lower aquatic organisms and these contain the largest amounts of OM.
- (2) Spatial distribution of OM can be accurately determined by combining logging geochemical models, M/S ratios, and OM accumulation models within the sequence stratigraphic framework. In the western region of the Fushan Depression, the occurrence of high-quality source rocks with abundant OM is limited to areas on the southern slope (SQIs3), the central part of the Huangtong Sag (SQIs2), and the northern part of the Huangtong Sag (SQIs1).
- (3) The method proposed in this study is suitable for source rock surveys in other lacustrine basins with heterogeneous sediments, because it requires only a minimal amount of geochemical data, relying instead on M/S ratios, which are generally readily available.

Acknowledgments

This study was funded by the Hainan Fushan Oilfield Exploration and Development Company (2020-HNYJ-003). The authors are grateful to Lei Zhu and Shengbao Shi for their assistance with the geochemical analysis. We also acknowledge three anonymous reviewers for their valuable comments and suggestions, which greatly improve the manuscript of an earlier version.

Appendix A. Supplementary data

Supplementary data to this article can be found online at <https://doi.org/10.1016/j.petsci.2022.07.008>.

References

- Al-atta, M.A., Issa, G.I., Ahmed, M.A., et al., 2014. Source rock evaluation and organic geochemistry of belayim marine oil field, gulf of suez, Egypt. *Egypt. J. Petrol.* 23, 285–302. <https://doi.org/10.1016/j.ejpe.2014.08.005>.
- Bai, Y., Tan, M., 2020. Dynamic committee machine with fuzzy-c-means clustering for total organic carbon content prediction from wireline logs. *Comput. Geosci.* 146, 104626. <https://doi.org/10.1016/j.cageo.2020.104626>.
- Bodin, S., Fröhlich, S., Boutib, L., et al., 2011. Early toarcian source-rock potential in the central high atlas basin (central Morocco): regional distribution and depositional model. *J. Petrol. Geol.* 34, 345–363. <https://doi.org/10.1111/j.1747-5457.2011.00509.x>.
- Bordenave, M.L., Espitalié, J., Leplat, P., et al., 1993. Screening techniques for source rock evaluation. In: Bordenave, M.L. (Ed.), *Applied Petroleum Geochemistry*. Editions Technip, Paris, pp. 218–278.
- Bohacs, K.M., Carroll, A.R., Neal, J.E., et al., 2000. Lake-basin type, source potential, and hydrocarbon character: an integrated sequence-stratigraphic geochemical framework. *AAPG Stud. Geol.* 46, 3–34. <https://doi.org/10.1306/St46706C1>.
- Bourbonniere, R.A., Meyers, P.A., 1996. Sedimentary geolipid records of historical changes in the watersheds and productivities of Lakes Ontario and Erie. *Limnol. Oceanogr.* 41, 352–359. <https://doi.org/10.4319/lo.1996.41.2.0352>.
- Carroll, A.R., Bohacs, K.M., 1999. Stratigraphic classification of ancient lakes: balancing tectonic and climatic controls. *Geology* 27, 99–102. [https://doi.org/10.1130/0091-7613\(1999\)027<0099:SCOALB>2.3.CO;2](https://doi.org/10.1130/0091-7613(1999)027<0099:SCOALB>2.3.CO;2).
- Damsté, J.S.S., Kenig, F., Koopmans, M.P., et al., 1995. Evidence for gammacerane as an indicator of water column stratification. *Geochem. Cosmochim. Acta* 59, 1895–1900. [https://doi.org/10.1016/0016-7037\(95\)00073-9](https://doi.org/10.1016/0016-7037(95)00073-9).
- Demailon, G.J., Moore, G.T., 1980. Anoxic environments and oil source bed genesis. *Org. Geochem.* 2 (1), 9–31. [https://doi.org/10.1016/0146-6380\(80\)90017-0](https://doi.org/10.1016/0146-6380(80)90017-0).
- Eglinton, G., Hamilton, R.J., 1967. Leaf epicuticular waxes. *Science* 156, 1322–1335. <https://doi.org/10.1126/science.156.3780.1322>.
- Feng, Z., 2004. Single factor analysis and multifactor comprehensive mapping method: reconstruction of quantitative lithofacies palaeogeography.

- J. *Palaeogeogr.* 6, 3–19 (in Chinese with English abstract).
- Fertl, W., Chilingar, G., 1988. Total organic carbon content determined from well logs. *SPE Form. Evaluation* 3 (2), 407–419. <https://doi.org/10.2118/15612-PA>.
- Fu, C., Li, S., Li, S., et al., 2022. Genetic types of mudstone in a closed-lacustrine to open-marine transition and their organic matter accumulation patterns: a case study of the Paleocene source rocks in the east China sea basin. *J. Pet. Sci. Eng.* 208, 109343. <https://doi.org/10.1016/j.petrol.2021.109343>.
- Gagosian, R.B., Smith, S.O., Lee, C., et al., 1980. Steroid transformation in recent marine sediments. *Adv. Org. Geochem.* 407–419. [https://doi.org/10.1016/0079-1946\(79\)90122-8](https://doi.org/10.1016/0079-1946(79)90122-8).
- Gan, H., Wang, H., Shi, Y., et al., 2020. Geochemical characteristics and genetic origin of crude oil in the fushansag, Beibuwan Basin, south China sea. *Mar. Petrol. Geol.* 112, 104114. <https://doi.org/10.1016/j.marpetgeo.2019.104114>.
- Gomis, D.B., Fernandez, M.P., Gutiérrez Alvarez, M.D., 2000. Simultaneous determination of fat-soluble vitamins and pro-vitamins in milk by microcolumn liquid chromatography. *J. Chromatogr. A* 891, 109–114. [https://doi.org/10.1016/S0021-9673\(00\)00623-3](https://doi.org/10.1016/S0021-9673(00)00623-3).
- Grantham, P.J.P., Baak, A., 1983. *Triterpanes in a number of Far-Eastern crude oils*. In: BJORØY, M., ALBRECHT, P., CORNFORD, C., DE GROOT, K., EGLINTON, G., GALIMOV, E., LEYTHAEUSER, D., PELET, R., RULLKÖTTER, J., SPEERS, G. (Eds.), *Advances in Organic Geochemistry 1981*. Wiley, Chichester, pp. 675–683.
- Hartmann, M.A., 1998. Plant sterols and the membrane environment. *Trends Plant Sci.* 3, 170–175. [https://doi.org/10.1016/S1360-1385\(98\)01233-3](https://doi.org/10.1016/S1360-1385(98)01233-3).
- Hao, F., Zhou, X., Zhu, Y., et al., 2011. Lacustrine source rock deposition in response to co-evolution of environments and organisms controlled by tectonic subsidence and climate, Bohai Bay Basin, China. *Org. Geochem.* 42, 323–339. <https://doi.org/10.1016/j.orggeochem.2011.01.010>.
- Haven, H.L.T., Rullkötter, J., 1988. The diagenetic fate of taraxer-14-ene and oleanane isomers. *Geochim. Cosmochim. Acta* 52, 2543–2548. [https://doi.org/10.1016/0016-7037\(88\)90312-2](https://doi.org/10.1016/0016-7037(88)90312-2).
- Huang, W.Y., Meinschein, W.G., 1979. Sterols as ecological indicators. *Geochim. Cosmochim. Acta* 43, 739–745. [https://doi.org/10.1016/0016-7037\(79\)90257-6](https://doi.org/10.1016/0016-7037(79)90257-6).
- Hunt, J.M., 1996. *Petroleum Geochemistry and Geology*, second ed. W.H. Freeman and Company, New York, p. 743.
- Jiang, S., Chen, L., Wu, Y., et al., 2017. Hybrid plays of upper triassic Chang7 lacustrine source rock interval of yangchang formation, ordos basin, China. *J. Pet. Sci. Eng.* 159, 182–196. <https://doi.org/10.1016/j.petrol.2017.09.033>.
- Lai, H., Li, M., Liu, J., et al., 2020a. Source rock assessment within a sequence stratigraphic framework of the Yogou Formation in the Termit Basin, Niger. *Geol. J.* 55 (4), 2473–2494. <https://doi.org/10.1002/gj.3523>.
- Lai, H., Li, M., Liu, J., et al., 2018. Organic geochemical characteristics and depositional models of Upper Cretaceous marine source rocks in the Termit Basin, Niger. *Palaeogeogr. Palaeoclimatol. Palaeoecol.* 495, 292–308. <https://doi.org/10.1016/j.palaeo.2018.01.024>.
- Lai, H., Li, M., Liu, J., et al., 2020b. Source rock types, distribution and their hydrocarbon generative potential within the Paleogene Sokor-1 and LV formations in Termit Basin, Niger. *Energy Explor. Exploit.* 38 (6), 2143–2168. <https://doi.org/10.1177/0144598720915534>.
- Lai, H., Li, M., Jian, X., et al., 2020c. An integrated sequence stratigraphic–geochemical investigation of the Jurassic source rocks in the North Yellow Sea Basin, eastern China. *AAPG (Am. Assoc. Pet. Geol.) Bull.* 104 (10), 2145–2171. <https://doi.org/10.1306/05212019072>.
- Li, M., Lai, H., Mao, F., et al., 2018. Geochemical assessment of source rock within a stratigraphic geochemical framework: taking termit basin (Niger) as an example. *Earth Sci.* 43 (10), 3603–3615. <https://doi.org/10.3799/dqkx.2018.223> (in Chinese with English abstract).
- Li, Y., Lin, S., Wang, H., et al., 2017. Depositional setting analysis using seismic sedimentology: example from the Paleogene Liushagang sequence in the Fushan depression, South China Sea. *Geodesy Geodyn.* 8, 347–355. <https://doi.org/10.1016/j.geog.2017.05.001>.
- Li, M., Wang, T., Liu, J., et al., 2008. Occurrence and origin of carbon dioxide in the fushan depression, Beibuwan Basin, south China sea. *Mar. Petrol. Geol.* 25, 500–513. <https://doi.org/10.1016/j.marpetgeo.2007.07.007>.
- Li, J., Wang, R., Qin, J., et al., 2020. Paleogene-Neogene micropaleontological records of the Weixinan Depression, Beibuwan Basin and their paleoenvironmental significance. *Mar. Geol. Quat. Geol.* 40 (2), 29–36. <https://doi.org/10.16562/j.cnki.0256-1492.2019101901> (in Chinese with English abstract).
- Liao, F., Ma, Q., Sun, X., et al., 2015. Study of lithologic reservoir of paleogene Liushagang Formation in fushan depression of beibu Bay Basin. *China Pet. Explor.* 20 (2), 43–50. <https://doi.org/10.3969/j.issn.1672-7703.2015.02.005> (in Chinese with English abstract).
- Liu, B., Shi, J., Fu, X., et al., 2018. Petrological characteristics and shale oil enrichment of lacustrine fine-grained sedimentary system: a case study of organic-rich shale in first member of Cretaceous Qingshankou Formation in Gulong Sag, Songliao Basin, NE China. *Petrol. Explor. Dev.* 45 (5), 884–894. [https://doi.org/10.1016/S1876-3804\(18\)30091-0](https://doi.org/10.1016/S1876-3804(18)30091-0).
- Liu, E., Wang, H., Li, Y., et al., 2015. Relative role of accommodation zones in controlling stratigraphic variability and facies distribution: insights from the Fushan Depression, South China Sea. *Mar. Petrol. Geol.* 68, 219–239. <https://doi.org/10.1016/j.marpetgeo.2015.08.027>.
- Liu, E., Wang, H., Lin, Z., et al., 2012. Characteristics and hydrocarbon enrichment rules of transfer zone in Fushan Sag, Beibuwan Basin. *J. Cent. S. Univ.* 43 (10), 3946–3953 (in Chinese with English abstract).
- Liu, E., Wang, H., Li, Y., et al., 2014. Sedimentary characteristics and tectonic setting of sublacustrine fans in a half-graben rift depression, Beibuwan Basin, South China Sea. *Mar. Petrol. Geol.* 52, 9–21. <https://doi.org/10.1016/j.marpetgeo.2014.01.008>.
- Lu, Z., Gan, H., Shi, Y., et al., 2016. Geochemical characteristics of crude oil and oil-source correlation in the western fushan depression. *Earth Sci.* 41 (1), 111–122. <https://doi.org/10.3799/dqkx.2016.132> (in Chinese with English abstract).
- Luo, W., Xie, J., Liu, X., et al., 2013. The study of paleogene climate in the haizhong depression, Beibuwan Basin, northern south China sea. *Acta Micropaleontol. Sin.* 30 (3), 288–296 (in Chinese with English abstract).
- Løseth, H., Wensaas, L., Gading, M., et al., 2011. Can hydrocarbon source rocks be identified on seismic data? *Geology* 39 (12), 1167–1170. <https://doi.org/10.1130/G32328.1>.
- Ma, Q., Zhao, S., Liao, Y., et al., 2012. Sequence architectures of paleogene Liushagang Formation and its significance in fushan sag of the Beibuwan Basin. *Earth Sci. J. China Univ. Geosci.* 37 (4), 667–678. <https://doi.org/10.3799/dqkx.2012.076> (in Chinese with English abstract).
- Magoon, L.B., 2004. Petroleum system: nature's distribution system for oil and gas. *Encycl. Energy* 823–836. <https://doi.org/10.1016/b0-12-176480-x/00251-5>.
- Mahmoud, A.A.A., Elkhatatny, S., Mahmoud, M., et al., 2017. Determination of the total organic carbon (TOC) based on conventional well logs using artificial neural network. *Int. J. Coal Geol.* 179, 72–80. <https://doi.org/10.1016/j.coal.2017.05.012>.
- Makled, W.A., Mostafa, T.F., Mousa, D.A., et al., 2018. Source rock evaluation and sequence stratigraphic model based on the palynofacies and geochemical analysis of the subsurface Devonian rocks in the Western Desert, Egypt. *Mar. Petrol. Geol.* 89, 560–584. <https://doi.org/10.1016/j.marpetgeo.2017.10.021>.
- Meyers, P.A., 1997. Organic geochemical proxies of paleoceanographic, paleolimnologic, and paleoclimatic processes. *Org. Geochem.* 27, 213–250. [https://doi.org/10.1016/S0146-6380\(97\)00049-1](https://doi.org/10.1016/S0146-6380(97)00049-1).
- Moldowan, J.M., Dahl, J., Huizinga, B.J., et al., 1994. The molecular fossil record of oleanane and its relation to angiosperms. *Science* 265, 768–771. <https://doi.org/10.1126/science.265.5173.768>.
- Moldowan, J.M., Seifert, W.K., Gallegos, E.J., 1985. Relationship between petroleum composition and depositional environment of petroleum source rock. *Ame. Ass. Petrol. Geol.* 69, 1255–1268. <https://doi.org/10.1306/AD462BC8-16F7-11D7-8645000102C1865D>.
- Mort, H., Jacquet, O., Adatte, T., et al., 2007. The Cenomanian/Turonian anoxic event at the Bonarelli Level in Italy and Spain: enhanced productivity and/or better preservation. *Cretac. Res.* 28 (4), 597–612. <https://doi.org/10.1016/j.cretres.2006.09.003>.
- Ndip, E.A., Agyingi, C.M., Nton, M.E., et al., 2019. Organic petrography and petroleum source rock evaluation of the Cretaceous Mamfe Formation, Mamfe basin, southwest Cameroon. *Int. J. Coal Geol.* 202, 27–37. <https://doi.org/10.1016/j.coal.2018.11.005>.
- Passy, Q., Creaney, S., Kulla, J., et al., 1990. A practical model for organic richness from porosity and resistivity logs. *AAPG Bull.* 74, 1777–1794. <https://doi.org/10.1306/0C9B25C9-1710-11D7-8645000102C1865D>.
- Pedersen, T.F., Calvert, S.E., 1990. Anoxia vs. Productivity: what controls the formation of organic-carbon-rich sediments and sedimentary rocks. *AAPG Bull.* 74 (4), 454–466. <https://doi.org/10.1306/0C9B232B-1710-11D7-8645000102C1865D>.
- Peters, K.E., 1986. Guidelines for evaluating petroleum source rock using programmed pyrolysis. *AAPG (Am. Assoc. Pet. Geol.) Bull.* 70, 318–329. <https://doi.org/10.1306/94885688-1704-11D7-8645000102C1865D>.
- Peters, K.E., Cassa, M.R., 1994. *Applied source rock geochemistry*. In: Magoon, L.B., Dow, W.G. (Eds.), *The Petroleum System-From Source to Trap*, vol. 60. AAPG Memoir, pp. 93–115.
- Peters, K.E., Moldowan, J.M., 1991. Effects of source, thermal maturity, and biodegradation on the distribution and isomerization of homohopanes in petroleum. *Org. Geochem.* 17, 47–61. [https://doi.org/10.1016/0146-6380\(91\)90039-M](https://doi.org/10.1016/0146-6380(91)90039-M).
- Peters, K.E., Moldowan, J.M., 1993. *The Biomarker Guide: Interpreting Molecular Fossils in Petroleum and Ancient Sediments*. Prentice-Hall, Inc, Englewood Cliffs, New Jersey.
- Peters, K.E., Snedden, J.W., Sulaeman, A., et al., 2000. A new geochemical-sequence stratigraphic model for the mahakam delta and makassar slope, kalimantan, Indonesia. *AAPG (Am. Assoc. Pet. Geol.) Bull.* 84 (1), 12–44. <https://doi.org/10.1306/C9EBDC51-1735-11D7-8645000102C1865D>.
- Peters, K.E., Walters, C.C., Moldowan, J.M., 2005. *The Biomarker Guide: Biomarkers and Isotopes in Petroleum Exploration and Earth History*, second ed., vol. 2. Cambridge University Press, Cambridge.
- Sageman, B.B., Murphy, A.E., Werne, J.P., et al., 2003. A tale of shales: the relative roles of production, decomposition, and dilution in the accumulation of organic-rich strata, Middle–Upper Devonian, Appalachian basin. *Chem. Geol.* 195 (1–4), 229–273. [https://doi.org/10.1016/S0009-2541\(02\)00397-2](https://doi.org/10.1016/S0009-2541(02)00397-2).
- Schmoker, J., 1979. Determination of organic content of Appalachian Devonian shales from formation-density logs. *AAPG Bull.* 63 (9), 1504–1509. <https://doi.org/10.1306/2F9185D1-16CE-11D7-8645000102C1865D>.
- Shanmugam, G., 1985. Significance of coniferous rain forests and related organic matter in generating commercial quantities of oil, Gippsland basin, Australia. *AAPG Bull.* 69, 1241–1254. <https://doi.org/10.1306/AD462BC3-16F7-11D7-8645000102C1865D>.
- Sheikh, H.E., Faris, M., Shaker, F., et al., 2016. Mineralogy and source rock evaluation of the marine Oligo-Miocene sediments in some wells in the Nile Delta and North Sinai, Egypt. *J. Afr. Earth Sci.* 118, 163–173. <https://doi.org/10.1016/j.jafrearsci.2016.03.001>.

- Shi, Y., Guo, H., Liao, F., et al., 2020. Physical properties and geochemical characteristics of crude oil in Fushan Sag, Beibuwan Basin. *China Offshore Oil Gas* 32 (6), 31–42. <https://doi.org/10.11935/j.issn.1673-1506.2020.06.004> (in Chinese with English abstract).
- Smith, D.J., Englinton, G., Morris, R.J., et al., 1982. Aspect of the steroid geochemistry of recent diatomaceous sediment from the Namibian shelf. *Oceanol. Acta* 5, 365–378.
- Surdam, R.O., Staley, K.O., 1979. Lacustrine sedimentation during the culminating phase of Eocene lake gosiute, Wyoming (green river formation). *Geol. Soc. Am. Bull.* 90, 93–110. [https://doi.org/10.1130/0016-7606\(1979\)90<93:LSDTCP>2.0.CO;2](https://doi.org/10.1130/0016-7606(1979)90<93:LSDTCP>2.0.CO;2).
- Tissot, B.P., Welte, D.H., 1984. *Petroleum Formation and Occurrence (Second Revised and Enlarged Edition)*. Springer-Verlag, Berlin, pp. 495–546.
- Volk, H., George, S.C., Middleton, H., et al., 2005. Geochemical comparison of fluid inclusion and present-day oil accumulations in the Papuan Foreland—evidence for previously unrecognised petroleum source rocks. *Org. Geochem.* 36, 29–51. <https://doi.org/10.1016/j.orggeochem.2004.07.018>.
- Volkman, J.K., Barrett, S., Blackburn, S.I., 1999. Eustigmatophyte microalgae are potential source of C₂₉ sterols, C₂₂–C₂₈ n-alcohols and C₂₈–C₃₂ n-alkyl diols in freshwater environments. *Org. Geochem.* 30, 307–318. [https://doi.org/10.1016/S0146-6380\(99\)00009-1](https://doi.org/10.1016/S0146-6380(99)00009-1).
- Volkman, J.K., Maxwell, J.R., 1986. Acyclic isoprenoids as biological markers. In: Johns, R.B. (Ed.), *Biological Markers in the Sedimentary Record*. Elsevier, New York, pp. 1–42.
- Wang, P., Chen, Z., Pang, X., et al., 2016. Revised models for determining TOC in shale play: example from devonian duvernay shale, western Canada sedimentary basin. *Mar. Petrol. Geol.* 70, 304–319. <https://doi.org/10.1016/j.marpetgeo.2015.11.023>.
- Wang, H., Wu, W., Chen, T., et al., 2019. An improved neural network for TOC, S1 and S2 estimation based on conventional well logs. *J. Pet. Sci. Eng.* 176, 664–678. <https://doi.org/10.1016/j.petrol.2019.01.096>.
- Xu, J., Jin, Q., Xu, X., et al., 2021. Factors controlling organic-rich shale development in the Liushagang Formation, weixinan sag, beibu gulf basin: implications of structural activity and the depositional environment. *Petrol. Sci.* 18, 1011–1020. <https://doi.org/10.1016/j.petsci.2020.08.001>.
- Yin, J., Xu, C., Hao, F., et al., 2020. Controls on organic matter enrichment in source rocks of the shahejie Formation in the southwestern Bozhong sag, Bohai Bay Basin, China. *Palaeogeogr. Palaeoclimatol. Palaeoecol.* 560, 110026. <https://doi.org/10.1016/j.palaeo.2020.110026>.
- Yu, H., Rezaee, R., Wang, Z., et al., 2017. A new method for TOC estimation in tight shale gas reservoirs. *Int. J. Coal Geol.* 179, 269–277. <https://doi.org/10.1016/j.coal.2017.06.011>.
- Zeng, B., Li, M., Zhu, J., et al., 2021. Selective methods of TOC content estimation for organic-rich interbedded mudstone source rocks. *J. Nat. Gas Sci. Eng.* 93 (5), 104064. <https://doi.org/10.1016/j.jngse.2021.104064>.
- Zhang, Z., Liu, Z., Zhang, G., et al., 2013. The chasmic stage and structural evolution features of Beibuwan Basin. *J. Oil Gas Technol. (J. Jiangnan Petroleum Inst.)* 35 (1), 6–10+172 (in Chinese with English abstract).
- Zou, Y., Sun, J., Li, Z., et al., 2018. Evaluating shale oil in the Dongying Depression, Bohai Bay Basin, China, using the oversaturation zone method. *J. Pet. Sci. Eng.* 161, 291–301. <https://doi.org/10.1016/j.petrol.2017.11.059>.